Received: 16 February 2021 | Revised: 3 June 2021 | Accepted: 4 August 2021

DOI: 10.1002/jdn.10146

RESEARCH ARTICLE

INTERNATIONAL JOURNAL OF DEVELOPMENTAL NEUROSCIENCE

ISDN WILEY

Cortical thickness in clinical moyamoya disease: A magnetic resonance imaging study

Grace Tompkins[1] | **Jacob Levman**[2] | **Prahar Ijner**[2] | **Tadashi Shiohama**[3] | **Emi Takahashi**[4,5]

[1]Department of Mathematics and Statistics, St. Francis Xavier University, Antigonish, Nova Scotia, Canada

[2]Department of Computer Science, St. Francis Xavier University, Antigonish, Nova Scotia, Canada

[3]Department of Pediatrics, Graduate School of Medicine, Chiba University, Chiba, Japan

[4]Division of Newborn Medicine, Department of Medicine, Boston Children's Hospital, Boston, MA, USA

[5]Department of Pediatrics, Harvard Medical School, Boston, MA, USA

Correspondence
Jacob Levman, Canada Research Chair in Bioinformatics, St. Francis Xavier University, Antigonish B2G 2W5, NS, Canada.
Email: jlevman@stfx.ca

Funding information
Natural Science and Engineering Research Council of Canada Discovery Grant, Grant/Award Number: R0192004; Nova Scotia Research and Innovation Trust, Grant/Award Number: R0176004; St. Francis Xavier University, Grant/Award Number: R0168020; Canada Foundation for Innovation; Natural Science and Engineering Research Council of Canada's Canada Research Chair, Grant/Award Number: 231266; National Institutes of Health, Grant/Award Numbers: HD098606, R01HD078561, R03NS091587, R21MH118739

Abstract

Moyamoya disease (MMD) is a progressive cerebrovascular disorder, with an unknown pathogenesis and aetiology. MMD is characterized by steno-occlusive changes at the terminal portion of the internal carotid artery (ICA), which is accompanied by variable development of the basal collaterals, also known as moyamoya vessels. Patients with MMD show variable patterns of brain damage and may experience recurrent multiple transient ischaemic attacks, intracranial bleeding and cerebral infarction. In this study, we investigate the potential for structural T1 magnetic resonance imaging (MRI) to help characterize abnormal cortical development in MMD clinically, with an analysis of both average and variability of regional cortical thicknesses. This study also included a machine learning analysis to assess the predictive capacity of the cortical thickness abnormalities observed in this research. This study included 993 MRI examinations from neurotypical controls and 269 MRI examinations from MMD patients. Results demonstrate abnormal cortical presentation of the insula, caudate, postcentral, precuneus and cingulate regions, in agreement with previous literature cortical thickness findings as well as alternative methods such as functional MRI (fMRI) and digital angiography. To the best of our knowledge, this is the first manuscript to report cortical thickness abnormalities in the middle temporal visual area in MMD and the first study to report on cortical thickness variability abnormalities in MMD.

List of abbreviations: ANNSoft, artificial neural network; BCH, Boston Children's Hospital; DT, decision tree; eTIV, estimated total intracranial volume; fMRI, functional magnetic resonance imaging; GM, grey matter; ICA, internal carotid artery; ICAD, intracranial atherosclerotic disease; LS, least squares prediction using bootstrap aggregation; MMD, moyamoya disease; MPRAGE, magnetization prepared rapid gradient echo; MRI, magnetic resonance imaging; OA, overall accuracy; RF, random forest; SVM, support vector machine; T1, longitudinal relaxation structural MRI; TIA, transient ischaemic attack.

KEYWORDS
cortical thickness, machine learning, magnetic resonance imaging, moyamoya, paediatric

1 | INTRODUCTION

Moyamoya disease (MMD) is a progressive cerebrovascular disorder that causes speech impairment, sensory and cognitive issues, motor control issues, disturbed consciousness and vision problems (Ganesan, 2010). Moyamoya was first described in 1957 when symptoms of cerebral infarction were found with hypoplasia of the internal carotid arteries in a Japanese population (Smith, 2015). The disease was named after the distinct appearance of cerebral vessels in an angiogram, which resemble a puff of smoke or 'moyamoya' in Japanese. Moyamoya's pathogenesis, which remains unclear, is multifactorial, including both genetic and environmental factors (Ganesan, 2010). MMD is characterized by stenoocclusive changes at the terminal portion of the internal carotid artery (ICA), which is accompanied by variable development of the basal collaterals, referred to as moyamoya vessels. Moyamoya vessels are formed to compensate for reduced blood supply due to the narrowing of the ICA; however, they stop functioning with time. These moyamoya vessels are often observed in the proximal portions of the middle and anterior cerebral arteries (Yamada, Himeno, et al., 1995). Patients with MMD show different patterns of brain damage and may experience recurrent multiple transient ischaemic attacks (TIAs), intracranial bleeding and cerebral infarction (Chaudhuri et al., 1993; Qiao et al., 2017). Some patients manifest complex clinical behaviour including epilepsy, headaches and a combination of motor, speech, visual, sensory and cognitive dysfunction (Duan et al., 2012; Suzuki & Kodama, 1983). Children also often experience muscular weakness or paralysis of one side of the body, and the first symptom of moyamoya is usually TIA or stroke in a paediatric population (Kim et al., 2010). The first symptom in adults is intracranial haemorrhaging in half of cases (Kuroda & Houkin, 2008).

Structural magnetic resonance imaging (MRI) has been used to study MMD to understand changes in cortical thicknesses, differentiate between MMD and intracranial atherosclerosis and to increase the accuracy of MMD diagnoses (Qiao et al., 2017; Sawada et al., 2012; Zaharchuk et al., 2011). Conventional angiographic evaluation methods cannot differentiate MMD from conditions such as intracranial atherosclerotic disease (ICAD) because it focuses only on the vessel lumen (Kim et al., 2013). In a study of 30 patients, all participants studied had bilateral occlusion or stenosis of the supraclinoid ICA and proximal anterior and middle cerebral arteries, which were clearly shown by MRI, and their findings demonstrated that MRI was useful in differentiating MMD from ICAD (Yamada, Suzuki, & Matsushima, 1995). Additionally, the use of MRI facilitates observations of vessel wall pathology, unlike conventional arterial imaging (Qiao et al., 2017). These findings are consistent with previous pathological reports, providing support for MRI potentially being helpful in differentiating ICAD from MMD (Kim et al., 2013), and research has suggested that cortical thickness may be an important biomarker for MMD (Qiao et al., 2017). Automated analysis tools such as FreeSurfer (Fischl, 2012) have been used extensively in the scientific literature to analyse structural MRIs in order to extract biomarkers from examinations localized to subregions of the patient's brain presentation. Both healthy subjects and subjects with various neurological conditions, including autism, multiple sclerosis, Alzheimer's disease and schizophrenia, have been studied with FreeSurfer (Deppe et al., 2016; Kong et al., 2012; Levman et al., 2017, 2018; Salat et al., 2012). Automated analysis tools have also been used more recently to characterize cortical thickness abnormalities in adult MMD patients (Lee et al., 2018; Qiao et al., 2017).

Since its description by Takeuchi and Shimizu (Suzuki & Takaku, 1969), extensive research including pathological, genetic, and angiography studies have been carried out to understand the aetiology/pathogenesis of, and neurological changes associated with MMD. The scientific literature has included reports of reduced cortical thicknesses in MMD patients (Lee et al., 2018; Qiao et al., 2017). In this study, we used T1-weighted MR images to assess regional grey matter (GM) abnormalities in 269 examinations from paediatric patients with MMD by comparing them to the measurements from 993 MRI examinations from control participants. We hypothesize that thorough assessment of a large clinical population of MRI examinations will contribute to the body of data acquired and thus improve our collective understanding of the clinical presentation of paediatric MMD. We also hypothesize that regional cortical thickness variability may help improve characterization of changes in the brains of patients with MMD and may represent biomarkers with the potential to assist in the assessment and characterization of brain development from MRI examinations. Finally, we hypothesize that it is possible to clinically validate previous MMD literature findings

with large-scale real-world clinical MRI examinations in a paediatric population.

2 | MATERIALS AND METHODS

2.1 | Participants

This retrospective study involved data from Boston Children's Hospital's (BCH) clinical imaging database, which was reviewed from 1 January 2009, to 24 February 2016, following ethics approval by the Institutional Review Board at BCH. Examinations were accessed through the Children's Research Integration System (Pienaar et al., 2014). Examinations of low quality (metal artefacts from dental fixtures, lack of volumetric structural T1-weighted examinations, motion artefacts, etc.) were excluded from this study. Examinations that were inaccessible due to technical reasons were also excluded from the study. Neurotypical control participants were identified retrospectively in a previous study as having a normal MRI examination as assessed by a BCH neuroradiologist (Levman et al., 2017), and no neurodevelopmental disorders indicated in their electronic patient medical records. Participants with an indication in their medical records of neurological problems including but not limited to cerebral palsy, traumatic brain injury, developmental delay, tuberous sclerosis complex, autism, stroke, neurofibromatosis, cortical dysplasia, epilepsy, multiple sclerosis and attention deficit hyperactivity disorder were excluded from the neurotypical cohort of this study. To avoid anomalous growth patterns affected by radiation and drug treatments, patients diagnosed with any form of cancer were also excluded from the neurotypical group. Patients with MMD were identified based on an indication of MMD in their electronic patient medical record. This resulted in 993 neurotypical and 269 MMD examinations, which were included for further analysis. The participant's age at the time of the examinations ranged between 0 and 38 years for the MMD population and between 0 and 31 years for the neurotypical cohort. The age distribution of the included participants is provided in the histogram in Figure 1. This represents a cross-sectional retrospective analysis of all patients identified with MMD across the review period.

2.2 | MRI data acquisition and preprocessing

This study involved T1-weighted structural volumetric examinations obtained from subjects imaged with three Tesla MRI scanners (Skyra, Siemens Medical Systems, Erlangen, Germany) at BCH. The retrospective nature of this study led to variability in the pulse sequences used to attain these T1-weighted structural volumetric images, which included numerous MPRAGE acquisitions, some volumetric spoiled gradient recalled sequences and traditional T1-weighted structural sequences. The average spatial resolution was approximately 1 mm, though there was variation in spatial resolution. Examinations were excluded if manual visual inspection observed patient motion artefacts. FreeSurfer's recon-all command (Fischl, 2012) was used to process the T1-weighted structural examinations. All available cortical thickness measurements (regionally distributed), including both average (mean) cortical thickness and variability of cortical thickness (as assessed by the standard deviation), were included for further analysis. This resulted in

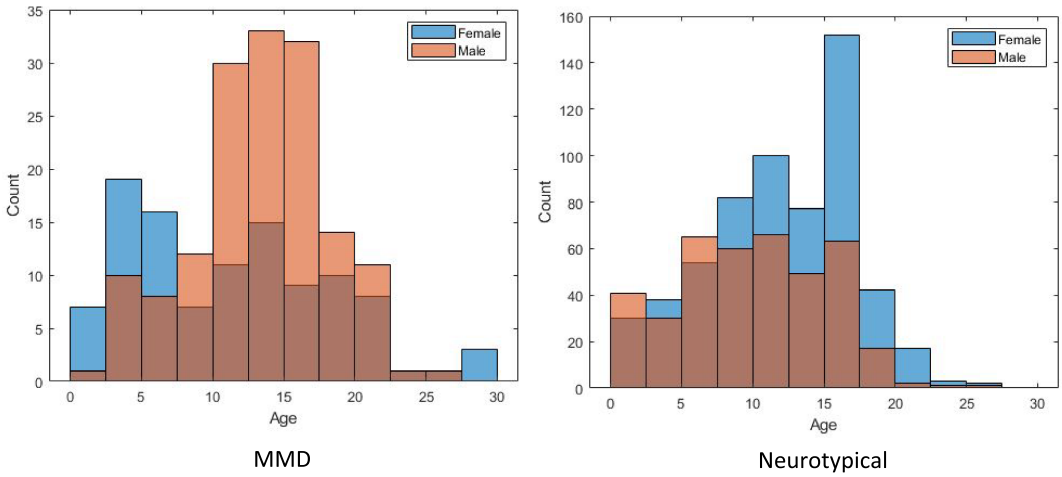

FIGURE 1 Age distribution of all participants examined. Left: 993 healthy participants (593 females, 395 males). Right: 269 MMD patients (112 females, 157 males)

662 measurements of cortical thickness extracted from each patient examination by FreeSurfer (Fischl, 2012), including both average and variability of cortical thickness in each supported subregion. As group-wise differences of these clinically acquired measurements are of interest; each measurement was compared in a group-wise manner (with moyamoya compared with neurotypical patients) by using Cohen's *d* statistic. A positive Cohen's d statistic indicates a higher average value in the moyamoya population relative to the neurotypicals, whereas a negative *d* statistic indicates a lower average value in the moyamoya population.

Participants were divided into four groups based on age: early childhood (0–5 years old), late childhood (5–10 years old), early adolescence (10–15 years old) and late adolescence (15–20 years old). Patients aged 20 years of age and older were excluded from age-grouped analysis due to small sample size. This resulted in 662 extracted measurements per age group or a total of $m = 662 * 4 = 2648$ comparisons, yielding a multiple comparison corrected Bonferroni threshold for statistical significance of $p < 0.05/\mathrm{m} = 1.89\mathrm{e}^{-5}$.

A statistical model was constructed based on multivariable regression using MATLAB. Each measurement was adjusted for each age range in order to control for group differences in age, gender and estimated total intracranial volume (eTIV). This was used to evaluate whether differences observed between the MMD and neurotypical groups remained statistically significant after controlling for age, gender and eTIV. The primary findings reported in Tables 1–4 were calculated using the raw (unadjusted) data provided by FreeSurfer (Fischl, 2012) for ease of comparison with future studies.

2.3 | Machine learning

Following the statistical analysis, machine learning algorithms were compared using the same dataset of 269 neurotypical MRI examinations and 993 moyamoya-identified MRI examinations. Fifty randomized validation loops were used in the study of five different machine learning algorithms: artificial neural network (ANNSoft), support vector machine (SVM), decision tree (DT),

TABLE 1 Mean cortical thickness sorted by highest Cohen's *d*

Measurement type	0–5 years old L (d) R (d)	5–10 years old L (d) R (d)	10–15 years old L (d) R (d)	15–20 years old L (d) R (d)
Rostral anterior cingulate	L (−0.36841) R (−0.45608)	L (0.32125) R (0.16777)	L (−0.04208) R (0.099942)	L (0.40271) R (0.71373)
Inferior part of the precentral sulcus	L (0.17519) R (−0.03364)	L (0.14305) R (0.69694)	L (−0.28214) R (−0.34951)	L (−0.10971) R (−0.040894)
Cuneus	L (−0.074017) R (−0.1187)	L (0.52896) R (0.094328)	L (0.23539) R (−0.019366)	L (0.68746) R (0.42907)
Caudal anterior cingulate	L (−0.244) R (−0.0036315)	L (0.43826) R (0.27259)	L (0.12921) R (0.37729)	L (0.51993) R (0.68583)
Inferior segment of the circular sulcus of the insula	L (0.090605) R (−0.083572)	L (0.59623) R (0.5355)	L (0.34756) R (0.67312)	L (0.60428) R (0.29639)

TABLE 2 Mean cortical thickness sorted by lowest Cohen's *d*

Measurement type	0–5 years old L (d) R (d)	5–10 years old L (d) R (d)	10–15 years old L (d) R (d)	15–20 years old L (d) R (d)
Brodmann's middle temporal visual area	L (−0.28887) R (−0.66189)	L (−0.94317) R (−0.46789)	L (−0.57673) R (−0.11913)	L (−0.36804) R (−0.080466)
Superior frontal sulcus	L (−0.82193) R (−0.84788)	L (−0.38264) R (−0.30973)	L (−0.38406) R (−0.39712)	L (−0.51909) R (−0.19864)
Inferior parietal region	L (0.23698) R (−0.06768)	L (−0.55219) R (−0.80793)	L (−0.31107) R (−0.33638)	L (0.066106) R (0.020693)
Suborbital sulcus	L (−0.50596) R (−0.79232)	L (−0.077213) R (−0.42122)	L (−0.46854) R (−0.2468)	L (0.051342) R (0.10553)

TABLE 3 Standard deviation of cortical thickness sorted by highest Cohen's *d*

Measurement type	0–5 years old L (d) R (d)	5–10 years old L (d) R (d)	10–15 years old L (d) R (d)	15–20 years old L (d) R (d)
Insula	L (0.20348) R (0.58558)	L (0.55408) R (0.38054)	L (0.82793) R (0.69856)	L (0.97468) R (0.59457)
Pericallosal sulcus	L (−0.1579) R (−0.036778)	L (0.54283) R (0.30888)	L (0.39306) R (0.30742)	L (0.73749) R (0.88729)
Inferior segment of the circular sulcus of the insula	L (−0.35767) R (0.26858)	L (0.55469) R (0.40993)	L (0.74375) R (0.59348)	L (0.88499) R (0.38147)
Lateral aspect of the superior temporal gyrus	L (−0.22731) R (0.14226)	L (0.12003) R (0.48026)	L (0.38403) R (0.4575)	L (0.78051) R (0.43008)
Rostral anterior cingulate	L (0.104) R (0.25121)	L (−0.045247) R (0.23899)	L (0.18322) R (0.49815)	L (0.30035) R (0.74413)

TABLE 4 Standard deviation of cortical thickness sorted by lowest Cohen's *d*

Measurement type	0–5 years old L (d) R (d)	5–10 years old L (d) R (d)	10–15 years old L (d) R (d)	15–20 years old L (d) R (d)
Precuneus	L (−0.81648) R (−0.64172)	L (−0.32295) R (−0.34505)	L (−0.13026) R (−0.29009)	L (−0.17293) R (−0.34172)
Postcentral region	L (−0.79925) R (−0.38932)	L (−0.72386) R (−0.25374)	L (−0.45495) R (−0.47354)	L (−0.64573) R (−0.28222)
Inferior part of the precentral sulcus	L (−0.73114) R (−0.62547)	L (−0.48744) R (−0.46185)	L (−0.36645) R (−0.077385)	L (−0.26608) R (0.043447)
Inferior frontal sulcus	L (−0.7257) R (−0.36621)	L (−0.35882) R (−0.37997)	L (−0.16675) R (−0.2635)	L (−0.25642) R (0.10544)

random forest (RF), and least squares prediction using bootstrap aggregation (LS).

Randomization of the training and testing data consisted of assigning 50% of the participants to the training group and the remaining 50% to the testing group (hold-out validation). Randomization was done at the patient level as patients with multiple exams were to have all of their exams assigned to the same group of either training or testing data. Note that this can result in an imbalance of the number of examinations in each of the training and testing groups. Each of the five machine learning algorithms was randomly assigned the training data and then the model was tested with the randomly assigned testing data.

3 | RESULTS

Various regions of the brain demonstrated Bonferroni-corrected statistically significant differences in the GM cortical thickness measurements included in this analysis, potentially illustrating differences between neurotypical participants and those with MMD that may be associated with the condition. The leading results demonstrating the greatest group-wise differences are summarized in Tables 1–4. Tables 1–4 are sorted in decreasing order based on the largest magnitude of Cohen's *d* statistic observed at any age group.

Note that Table 2 is best suited to direct comparison with previous work investigating cortical thicknesses in MMD (Qiao et al., 2017), as this table is focused on the leading negative *d* statistics (MMD exhibits *reduced* mean cortical thickness) demonstrating group-wise differences based on average cortical thicknesses. Table 1 highlights those regions observed to have increased average cortical thicknesses in MMD, generally exhibiting smaller effect sizes than those observations from Table 2. Tables 3 and 4 present those regions observed to have abnormal cortical thickness variability (as assessed by the standard deviation). Thus, Tables 1, 3 and 4 represent findings not available in the current scientific literature. Table 2, while good for comparison, was compiled based on paediatric MMD patients, in contrast to the adult population studied previously in the literature (Qiao et al., 2017).

Table 5 provides the results of the five machine learning algorithms applied to this dataset in the context of

TABLE 5 Summary of randomization assessed overall accuracy across five machine learning algorithms

Algorithm	Mean overall accuracy	*SD* overall accuracy
LS	0.787572663	0.011443235
SVM	0.759727834	0.021536677
DT	0.648595126	0.022605299
RF	0.786653774	0.0115885
ANNSoft	0.787498603	0.010812485

Abbreviations: ANNSoft, artificial neural network; DT, decision tree; LS, least squares prediction using bootstrap aggregation; RF, random forest; SVM, support vector machine.

hold-out randomized validation. Validation was repeated, and the overall accuracy (OA) was reported for each randomized validation run and summarized statistically with the mean and standard deviation. Table 5 provides the average and standard deviation of the distribution of OA values for each machine learning technique as assessed across all randomized validation runs.

4 | DISCUSSION

In this study, we investigated the potential of regionally distributed cortical thickness measurements as biomarkers for assisting in characterizing MMD. This analytic approach helped identify a variety of brain regions exhibiting abnormal presentation of cortical thicknesses in MMD (such as the insula, the cuneus, the postcentral region and the middle temporal visual area). To the best of our knowledge, this is the first study to report abnormal reductions in average cortical thickness in Brodmann's middle temporal visual area, a finding that exhibited the strongest effect size in the left hemisphere and may be associated with known visual disturbances in MMD (Miyamoto et al., 1986; Noda et al., 1987). Abnormalities of the insula and the anterior cingulate identified in our study are supportive of functional MRI (fMRI) findings of reduced connectivity between the insula and the anterior cingulate (Kazumata et al., 2017). Our findings of reduced cortical thickness in the inferior parietal region and increased cortical thickness in the cingulate are supportive of previous research investigating the potential of diffusion MRI, whereby they found associations between functional characteristics and the presentation of the cingulate and inferior parietal regions (Kazumata et al., 2015). Additionally, our findings of abnormal presentation of the precuneus are supportive of previous findings based on functional MRI that identified those same regions as exhibiting altered functional connectivity (Kazumata et al., 2017). Additionally, our findings of abnormal presentation of the postcentral region are supportive of previous findings based on blood perfusion (Li et al., 2019). These regions and structures of the brain are involved with various cognitive functions. The insula is a brain structure that is involved with cognitive, affective and regulatory functions, which include awareness, emotional responses and empathic processes (Menon & Uddin, 2010). The precuneus is thought to play a central role in tasks including visuo-spatial imagery, episodic memory retrieval and self-processing operations (Cavanna & Trimble, 2006). Moyamoya causes speech impairment, sensory and cognitive issues, motor control issues, disturbed consciousness and vision problems, which are potentially consistent with the affected regions identified in this analysis.

Three of our evaluated machine learning approaches exhibited approximately equal predictive performance as assessed by the OA, including the ANNSoft, LS and the RF. The ANNSoft approach exhibited slightly smaller standard deviations, indicating it might be the most reliable approach in this task. Results demonstrate good predictive accuracy from all approaches except the DT, an antiquated technique provided for comparative purposes only. However, further work is needed to optimize a diagnostic test that makes use of the extensive cortical thickness measurements available from a program like FreeSurfer (Fischl, 2012). Statistical learning techniques provide promising research avenues towards contributing the next generation of diagnostic tools for MMD. It is hoped that by combining relevant information extractable from a standard T1 examination with biomarkers available from angiography, functional MRI and diffusion MRI, that machine learning can play a critical role in the thorough characterization of MMD on a per patient basis. Future work will look at multimodal integration facilitated by machine learning technologies. Machine learning can theoretically help physicians make informed decisions on diagnosis and flag patients who show some disease characteristics without having an official diagnosis. Additionally, patient care can be made more accessible and personalized as the technology is relatively inexpensive to implement.

There is no specific treatment to prevent MMD progression, though revascularization surgery is attempted to prevent stroke and restore adequate cerebral blood flow to underperfused regions (Berry et al., 2020; Shang et al., 2020). Surgical interventions for MMD have many options including the direct revascularization procedure, indirect revascularization procedure and the combined revascularization procedure. In the current clinical setting, adequate revascularization for MMD is selected according to several pieces of clinical information such as

clinical phase, onset age, area of ischaemia and the possible accompaniment of intracranial haemorrhage for each patient. The detailed analyses of cortical thicknesses in patients with MMD, such as in this study, potentially contribute to evaluating, in high resolution, developmental abnormalities that might be associated with mild hypo-perfusion not identified by single photon emission computed tomography, positron emission tomography or digital subtraction angiography. Additionally, cortical thicknesses may play a role as biomarkers for evaluating functional outcomes.

The main strength of this study was the large number of MRI examinations included, supporting as much statistical reliability in our analysis as we were able to accomplish (utilizing all available examinations available from the review period). The inclusion of cortical thickness variability as a biomarker of potential interest may assist in the characterization of brain development and growth patterns that may be related to the known abnormal cortical development previously observed in MMD. Weaknesses include the limited clinical information available about each patient, a compromise that was necessary to conduct a large-scale clinical study of this type. Information regarding which patients had undergone surgical intervention was not available for this analysis, and the period between the onset of clinical symptoms and MRI acquisition was also unknown. Future work will investigate the distribution of regional cortical thickness biomarkers across large datasets with a variety of different pulse sequences each being well represented in the dataset, a task that was not possible in the clinical MRI dataset used in this study. Future work will also investigate the approaches presented herein in the context of a prospective analysis with detailed clinical data for each patient, including neuropsychological data, information on the presence or absence of comorbid cognitive disorders and including a scale for assessing atrophy.

ACKNOWLEDGEMENTS

This work was supported by the National Institutes of Health (grant numbers R01HD078561, R21MH118739, HD098606 and R03NS091587) to ET; Natural Science and Engineering Research Council of Canada's Canada Research Chair grant (grant number 231266) to JL; a Canada Foundation for Innovation and Nova Scotia Research and Innovation Trust infrastructure grant (R0176004) to JL; a Natural Science and Engineering Research Council of Canada Discovery Grant (R0192004) to JL; and a St. Francis Xavier University research startup grant to JL (grant number R0168020).

CONFLICT OF INTEREST

The authors have no conflict of interest to report associated with this study.

ETHICS APPROVAL STATEMENT

This retrospective analysis was approved by the institutional review board (ethics board) of Boston Children's Hospital and ratified by St. Francis Xavier University.

PATIENT CONSENT STATEMENT

Patient consent was waived by the institutional review board at Boston Children's Hospital due to the lack of risk to the patients included in this retrospective analysis.

PERMISSION TO REPRODUCE MATERIALS FROM OTHER SOURCES

Not applicable.

AUTHOR CONTRIBUTIONS

JL conceived the analysis; JL and ET performed the supervision; JL, TS and GT did the manuscript authoring; GT, JL, TS and ET did the manuscript editing/approval; GT and PI performed the software development and review.

DATA AVAILABILITY STATEMENT

The data that support the findings of this study represent private clinical data from Boston Children's Hospital.

ORCID

Grace Tompkins https://orcid.org/0000-0003-4091-9970
Jacob Levman https://orcid.org/0000-0002-9604-3157
Prahar Ijner https://orcid.org/0000-0001-5447-9174
Tadashi Shiohama https://orcid.org/0000-0003-0076-5882

REFERENCES

Berry, J. A., Cortez, V., Toor, H., Saini, H., & Siddiqi, J. (2020). Moyamoya: An update and review. *Cureus*, *12*(10), e10994. https://doi.org/10.7759/cureus.10994

Cavanna, A., & Trimble, M. (2006). The precuneus: A review of its functional anatomy and behavioural correlates. *Brain*, *129*(3), 564–583. https://doi.org/10.1093/brain/awl004

Chaudhuri, R., Edwards, R., & Brooks, D. J. (1993). Adult moyamoya disease: An unusual cause of stroke. *British Medical Journal*, *307*(6908), 852–854.

Deppe, M., Tabelow, K., Krämer, J., Tenberge, J.-G., Schiffler, P., Bittner, S., Schwindt, W., Zipp, F., Wiendl, H., & Meuth, S. G. (2016). Evidence for early, non-lesional cerebellar damage in patients with multiple sclerosis: DTI measures correlate with disability, atrophy, and disease duration. *Multiple Sclerosis*, *22*, 73–84. https://doi.org/10.1177/1352458515579439

Duan, L., Bao, X.-Y., Yang, W.-Z., Shi, W.-C., Li, D.-S., Zhang, Z.-S., Zong, R., Han, C., Zhao, F., & Feng, J. (2012). Moyamoya

disease in China: Its clinical features and outcomes. *Stroke*, *43*, 56–60. https://doi.org/10.1161/STROKEAHA.111.621300

Fischl, B. (2012). FreeSurfer. *NeuroImage*, *62*(2), 774–781. https://doi.org/10.1016/j.neuroimage.2012.01.021

Ganesan, V. (2010). Moyamoya. *Journal of Pediatric Neurology*, *8*(1), 93–95.

Kazumata, K., Tha, K. K., Narita, H., Kusumi, I., Shichinohe, H., Ito, M., Nakayama, N., & Houkin, K. (2015). Chronic ischemia alters brain microstructural integrity and cognitive performance in adult moyamoya disease. *Stroke*, *46*(2), 354–360.

Kazumata, K., Tha, K. K., Uchino, H., Ito, M., Nakayama, N., & Abumiya, T. (2017). Mapping altered brain connectivity and its clinical associations in adult moyamoya disease: A resting-state functional MRI study. *PLoS ONE*, *12*(8), e0182759. https://doi.org/10.1371/journal.pone.0182759

Kim, S.-K., Cho, B. K., Phi, J. H., Lee, J. Y., Chae, J. H., Kim, K. J., Hwang, Y. S., Kim, I. O., Lee, D. S., Lee, J., & Wang, K. C. (2010). Pediatric moyamoya disease: An analysis of 410 consecutive cases. *Annals of Neurology*, *68*(1), 92–101. https://doi.org/10.1002/ana.21981

Kim, Y., et al. (2013). High resolution MRI differences between moyamoya disease and intracranial atherosclerosis. *European Journal of Neurology*, *20*(9), 1311–1318. https://doi.org/10.1111/ene.12202

Kong, L., Herold, C., Stieltjes, B., Essig, M., Seidl, U., Wolf, R. C., Wüstenberg, T., Lässer, M. M., Schmid, L. A., Schnell, K., Hirjak, D., & Thomann, P. A. (2012). Reduced gray to white matter tissue intensity contrast in schizophrenia. *PLoS ONE*, *7*, e37016. https://doi.org/10.1371/journal.pone.0037016

Kuroda, S., & Houkin, K. (2008). Moyamoya disease: Current concepts and future perspectives. *Lancet Neurology*, *7*(11), 1056–1066. https://doi.org/10.1016/S1474-4422(08)70240-0

Lee, J., Shimony, J. S., Jafri, H., Dacey, R. G., Zipfel, G. R., & Derdeyn, C. P. (2018). Hemodynamic impairment measured by positron-emission tomography is regionally associated with decreased cortical thickness in Moyamoya phenomenon. *American Journal of Neuroradiology*, *39*(11), 2037–2044. https://doi.org/10.3174/ajnr.A5812

Levman, J., MacDonald, P., Lim, A. R., Forgeron, C., & Takahashi, E. (2017). A pediatric structural MRI analysis of healthy brain development from newborns to young adults. *Human Brain Mapping*, *38*, 5931–5942. https://doi.org/10.1002/hbm.23799

Levman, J., Vasung, L., MacDonald, P., Rowley, S., Stewart, N., Lim, A., Ewenson, B., Galaburda, A., & Takahashi, E. (2018). Regional volumetric abnormalities in pediatric autism revealed by structural magnetic resonance imaging. *International Journal of Developmental Neuroscience*, *71*, 34–45. https://doi.org/10.1016/j.ijdevneu.2018.08.001

Li, J., Liu, X., Zhang, D., Zhang, Y., Wang, R., Yuan, J., & Zhao, J. (2019). Cognitive performance profile in pediatric moyamoya disease patients and its relationship with regional cerebral blood perfusion. *Frontiers in Neurology*, *10*, 1308. https://doi.org/10.3389/fneur.2019.01308

Menon, V., & Uddin, L. Q. (2010). Saliency, switching, attention and control: A network model of insula function. *Brain Structure and Function*, *214*(5), 655–667. https://doi.org/10.1007/s00429-010-0262-0

Miyamoto, S., Kikuchi, H., Karasawa, J., & Nagata, I. (1986). Visual disturbances in moyamoya disease. *Nō to Shinkei*, *38*(8), 765–772.

Noda, S., Hayasaka, S., Setogawa, T., & Matsumoto, S. (1987). Ocular symptoms of moyamoya disease. *American Journal of Ophthalmology*, *103*(6), 812–816. https://doi.org/10.1016/S0002-9394(14)74399-5

Pienaar R, Rannou N, Haehn D, Grant PE. ChRIS: real-time web-based MRI data collection analysis, and sharing. 20th Annual Meeting of the Organization for Human Brain Mapping (OHBM). 5. 2014.

Qiao, P.-G., Zuo, Z.-W., Han, C., Zhou, J., Hong-Tao, Z., Duan, L., Qian, T., & Gong-Jie, L. (2017). Cortical thickness changes in adult moyamoya disease assessed by structural magnetic resonance imaging. *Clinical Imaging*, *46*, 71–77. https://doi.org/10.1016/j.clinimag.2017.07.005

Salat, D. H., Williams, V. J., Leritz, E. C., Schnyer, D. M., Rudolph, J. L., Lipsitz, L. A., McGlinchey, R. E., & Milberg, W. P. (2012). Inter-individual variation in blood pressure is associated with regional white matter integrity in generally healthy older adults. *NeuroImage*, *59*(1), 181–192. https://doi.org/10.1016/j.neuroimage.2011.07.033

Sawada, T., Yamamoto, A., Miki, Y., Kikuta, K., Okada, T., Kanagaki, M., Kasahara, S., Miyamoto, S., Takahashi, J. C., Fukuyama, H., & Togashi, K. (2012). Diagnosis of moyamoya disease using 3-T MRI and MRA: Value of cisternal moyamoya vessels. *Neuroradiology*, *54*, 1089–1097. https://doi.org/10.1007/s00234-012-1020-1

Shang, S., Zhou, D., Ya, J., Li, S., Yang, Q., Ding, Y., Ji, X., & Meng, R. (2020). Progress in moyamoya disease. *Neurosurgical Review*, *43*(2), 371–382. https://doi.org/10.1007/s10143-018-0994-5

Smith, E. R. (2015). Moyamoya Biomarkers. *Journal of Korean Neurosurgical Society*, *6*(57), 415–421.

Suzuki, J., & Kodama, N. (1983). Moyamoya disease—A review. *Stroke*, *14*, 104–109. https://doi.org/10.1161/01.str.14.1.104

Suzuki, J., & Takaku, A. (1969). Cerebrovascular moyamoya disease: Disease showing abnormal net-like vessels in base of brain. *Archives of Neurology*, *20*, 288–299. https://doi.org/10.1001/archneur.1969.00480090076012

Yamada, I., Himeno, Y., Suzuki, S., & Matsushima, Y. (1995). Posterior circulation in moyamoya disease: Angiographic study. *Radiology*, *197*, 239–246. https://doi.org/10.1148/radiology.197.1.7568830

Yamada, I., Suzuki, S., & Matsushima, Y. (1995). Moyamoya disease: Diagnostic accuracy of MRI. *Diagnostic Neuroradiology*, *37*, 356–361. https://doi.org/10.1007/BF00588011

Zaharchuk, G., Do, H. M., Marks, M. P., Rosenberg, J., Moseley, M. E., & Steinberg, G. K. (2011). Arterial spin-labeling MRI can identify the presence and intensity of collateral perfusion in patients with moyamoya disease. *Stroke*, *42*, 2485–2491. https://doi.org/10.1161/STROKEAHA.111.616466

How to cite this article: Tompkins, G., Levman, J., Ijner, P., Shiohama, T., & Takahashi, E. (2021). Cortical thickness in clinical moyamoya disease: A magnetic resonance imaging study. *International Journal of Developmental Neuroscience*, *81*(8), 698–705. https://doi.org/10.1002/jdn.10146